# Stochastic dynamics of a rod bouncing upon a vibrating surface

H. S. Wright, Michael R. Swift, and P. J. King
*School of Physics and Astronomy, University of Nottingham, Nottingham, NG7 2RD, United Kingdom*
(Received 31 August 2006; published 27 December 2006)

We describe the behavior of a rod bouncing upon a horizontal surface which is undergoing sinusoidal vertical vibration. The predictions of computer simulations are compared with experiments in which a stainless-steel rod bounces upon a metal-coated glass surface. We find that, as the dimensionless acceleration parameter $\Gamma$ is increased appreciably above unity, the motion of a long rod passes from periodic or near-periodic motion into stochastic dynamics. Within this stochastic regime the statistics of the times between impacts follow distributions with tails of approximately Gaussian form while the probability distributions of the angles at impact have tails that are close to exponential. We determine the dependence of each distribution upon the length of the rod, upon frequency, and on $\Gamma$. The statistics of the total energy and of the translational and rotational components each approximately follow a Boltzmann distribution in their tails, the translational and rotational energy components being strongly correlated. The time-averaged mean vertical translational energy is significantly larger than the mean rotational energy, and both are considerably larger than the energy associated with horizontal motion.

DOI: 10.1103/PhysRevE.74.061309 PACS number(s): 45.05.+x, 45.70.−n

## I. INTRODUCTION

This paper concerns the motion of a rod bouncing upon a horizontal surface that is being vibrated in the vertical direction $z$ as $z(t)=a\sin(\omega t)$. In particular we consider the nature of the motion found when the reduced acceleration parameter $\Gamma=a\omega^2/g$ is substantially greater than unity. Here $g$ is the acceleration due to gravity. We shall examine in particular statistical aspects of the rod behavior.

The motion of a spherical ball bouncing upon a vertically vibrated surface has been studied extensively [1–7]. A ball, initially resting upon the surface, will be thrown from it if $\Gamma$ is greater than unity. It will then undergo bouncing behavior determined by $\Gamma$ and by the normal coefficient of restitution $e_n$ [8]. The explicit dependence on frequency can be removed by scaling all times by the period of vibration.

For low values of $e_n$, the sphere bounces once per cycle for values of $\Gamma$ just exceeding unity, and period-doubling bifurcations appear if $\Gamma$ is slowly increased. The motion may exhibit abrupt transitions into stochastic behavior at particular values of $\Gamma$, which depend upon $e_n$. For values of $e_n$ closer to unity the ball exhibits a single transition from a lower-$\Gamma$ bifurcation regime into stochastic motion which persists to higher $\Gamma$, save that in a limited number of narrow ranges of $\Gamma$ just above the transition, periodic behavior may be found [1,2,9,10].

Previous authors have derived an expression for the statistical distribution of energy of the bouncing ball in the fully stochastic regime. They suppose that, when $\Gamma$ is sufficiently large and $e_n$ is sufficiently close to unity, there is negligible correlation between the bouncing times of the ball and the phase of the platform motion [4,5,11]. It is then predicted that the probability $P(E)$ of the ball having a rebound energy $E$ will have a tail proportional to $\exp(-E/E_0)$, where $E_o \sim ma^2\omega^2/(1-e_n)$ and $m$ is the mass of the ball. While this result is broadly in line with experiment and with numerical simulation, some additional structure is observed in both [4,5]. This structure is due to partial correlation between the flight times between bounces and the vibration period. It is evident even at substantial amplitudes of vibration.

The bouncing ball is a simple example of an "impact oscillator." This class of strongly nonlinear system has mechanically driven components whose motion follows analytic equations. This motion is interrupted from time to time by abrupt impacts which map a preimpact set of system variables onto a new postimpact set. Many such systems have been studied, including driven beams, multiple coupled masses, or coupled pendulums that impact a rigid wall in their motion [12]. Few analytical results are known for the dynamics of many of these systems, particularly for statistical aspects of the motion, but they do share many common behaviors. As with a ball bouncing on a vibrated platform, these include periodic motion at low driving amplitudes, bifurcations at higher amplitudes, and the abrupt transitions into stochastic motion at critical amplitudes of excitation, sometimes the result of "crises" [10,13].

There is currently much interest in the bouncing behavior of nonspherical objects, for which the rotational motion and the vertical and horizontal motions of the center of mass are strongly coupled and for which length scales are important [14–19]. Large numbers of constrained rods moving on a vertical vibrated horizontal surface are known to show a rich variety of collective behaviors [17–19]. However, the behavior of single objects is also of interest. The low-energy dynamics of a single dimer consisting of two spheres joined by a rod have been studied in detail both in experiment and in simulation [15,16]. When dropped upon a vertically vibrated horizontal surface, such a dimer exhibits a number of distinct periodic modes at values of $\Gamma$ less than unity. In one of the modes the dimer bounces upon the surface without rotation. In another mode it bounces with alternating rotation so that the two spheres strike the surface in turn. In a third mode one sphere undergoes larger-amplitude vibrations than the other, the lower-amplitude sphere undergoing slip-stick motion. The dimer then moves horizontally across the surface. In each of these behaviors the angles involved are low and the dynamics occur almost entirely in two dimensions. It was

 

briefly noted that at values of $\Gamma$ above unity a vibrated dimer undergoes "complicated hopping and tumbling" [16].

Here we report the dynamics of single rods bouncing on a vibrated surface, principally studying the behavior for situations where $\Gamma$ is appreciably greater than unity. In the laboratory we observe that for some rod and surface materials the motion is close to two dimensional over many periods of vibration. For other systems the bouncing behavior shows tumbling appreciably involving the third dimension. Here, we restrict ourselves in experiment to a system consisting of a cylindrical stainless-steel rod vibrated upon a metal-coated glass surface, where the motion of the rod is effectively two dimensional.

We have used both experimentation and numerical simulation to study rod behavior. We observe that at values of $\Gamma$ comparable to unity a rod exhibits a range of periodic and near-periodic behaviors including those reported for dimers. However, at a threshold value of $\Gamma$, which depends only weakly upon the system parameters, the rod dynamics pass abruptly from these periodic or near-periodic motions to stochastic behavior. Above this threshold many features of the behavior may be approximately described by continuous statistical distributions of a simple form.

Simulations enable investigation of quantities that are not readily accessible to experimental measurement. However, the impact of a rod with a solid surface is far more difficult to model accurately than the impact of a sphere. A collision between a rod and a surface often excites flexural modes of the rod, and these may lead to a number of successive rod-surface impacts separated by very small intervals of time [20,21]. The collision cannot accurately then be treated as a single impact characterized by a small number of material parameters.

In attempting to fit experimental observations some authors have allowed model parameters such as $e_n$ to depend upon the angle at impact between the rod and surface [22]. Here we have used a two-dimensional molecular dynamics (MD) model, which treats the interaction between the rod and surface through damped springs, allowing slip with a single friction coefficient. We find that it offers an adequate description of the principal experimental observations when $e_n$ is suitably chosen. Comparison with experimental observations is used to justify use of the numerical model, and the model is then used to develop our understanding of the rod statistics.

## II. EXPERIMENTAL TECHNIQUES

The experiments were conducted using stainless steel rods of density 7900 $\mathrm{kgm}^{-3}$. They were of diameter $d$ equal to 1.0, 2.4, or 3.2 mm, and of lengths $L$ ranging from 6 to 24 mm in steps of about 3 mm. Rods were prepared with hemispherical ends having a radius of curvature of $d/2$, the surfaces being polished with a series of diamond pastes of grades down to 1 $\mu$m, making the surfaces optically smooth. The rods were vibrated on an 8-cm-diameter glass telescope mirror, having a radius of curvature of 0.8 m. This curvature is sufficient to retain the bouncing rods on the surface of the mirror and to ensure that the bouncing rods only impact the surface at their ends. The mirror is, however, sufficiently flat, on a length scale $d$, for the detailed dynamics to be little affected by the curvature.

It was observed that rods vibrated upon a bare glass surface were somewhat affected by the static charge that built up after extended periods of time. To eliminate such effects the mirror was coated by evaporation with a 0.5-$\mu$m-thick layer of Nichrome, which was then electrically grounded. Such a thin film is sufficiently hard not to be appreciably damaged by the impact of the rods.

The mirror was vibrated by attaching it to an electromagnetic transducer consisting of a coupled pair of long-throw loudspeakers, arranged to ensure accurate one-dimensional motion aligned within 0.2° of the vertical direction. The motion of the mirror was monitored using a capacitance acceleration sensor, while, in some parts of this study, the motion of the rods was observed using a high speed camera, usually operated at 1000 frames per second.

A piezoelectric transducer attached to the underside of the mirror was used to detect rod impacts with the mirror. The impulse signals were analyzed by a computer to yield information, such as the times between bounces, used in our analysis of rod statistics.

## III. NUMERICAL SIMULATIONS

We have performed a series of numerical simulations of the motion of a bouncing rod based on a simplified "soft-sphere" molecular dynamics technique [19,23,24], designed to capture the principal features of the motion. In this MD model a rod is treated as a cylinder of unit mass, of zero radius, of length $L$, and of moment of inertia given by $I=L^2/12$. Flexural modes of vibration are ignored. The rod is assumed to move in two dimensions, having two translational degrees and one rotational degree of freedom. In flight the motion of the rod is treated through the usual rules of Newtonian mechanics. During collisions between the ends of the rod and the vibrating plane surface, the normal forces are treated using a linear spring having spring constant $K_n=10^7\ \mathrm{N\ m}^{-1}$ [19]. A dashpot provides a damping force proportional to the normal component of the collision velocity. The damping is adjusted to give the experimental values of the coefficient of restitution discussed below. The tangential forces are treated in the following way. The end of the rod is subject to tangential forces provided by an undamped linear spring which is extended by the force. This linear spring has a spring constant of $K_t=10^9\ \mathrm{N\ m}^{-1}$. If the tangential force exceeds the normal force multiplied by a static coefficient of friction, then the contact slips, the tangential force then being the normal force multiplied by a kinetic coefficient of friction. In what follows we have set the two coefficients to be equal and have generally used the measured static coefficient of friction of $\mu=0.15$. The model allows for multiple slip-stick processes to occur.

Linear rather than Hertzian springs were selected following experimental measurements of the normal coefficient of restitution $e_n$ using a high-speed camera. Rods were dropped, and their bounce observed. They were aligned so that their principal axis remained vertical during the fall and first

TABLE I. The experimentally determined variation of the normal coefficient of friction with rod length, for polished stainless steel rods of 2.4 mm diameter with rounded ends. The methods used to determine $e_n$ (bounce) and $e_n$ (flip) are described in the text.

| Rod length (mm) | $e_n$ (bounce) | $e_n$ (flip) |
|---|---|---|
| 5.8 | 0.971±0.005 | 0.968±0.004 |
| 9.3 | 0.966±0.005 | 0.962±0.004 |
| 11.5 | 0.959±0.005 | 0.955±0.005 |
| 15.2 | 0.950±0.006 | 0.937±0.006 |
| 18.4 | 0.938±0.007 | 0.914±0.007 |
| 21.1 | 0.920±0.009 | 0.890±0.008 |

rebound. We found no significant variation of $e_n$ with initial height, as would be the case with Hertzian contacts. We did, however, note a systematic reduction of $e_n$ with increasing rod length. In our initial simulations we therefore used the measured value of $e_n$, $e_n$(bounce), appropriate to the particular length and diameter of the rod being simulated. Simulations were principally compared with experiments carried out on rods of diameter 2.4 mm, the $e_n$(bounce) for which are shown in Table I. The table also gives the measured rod lengths. Later we obtained a set of somewhat modified values, $e_n$(flip), also shown in Table I, by a technique that considers impacts having a distribution of impact angles. This technique is described below.

## IV. ROD DYNAMICS

### A. The onset of stochastic behavior

In experiment we observe a number of periodic and near-periodic motions at lower values of $\Gamma$, the behavior depending upon the past history of the frequency and $\Gamma$ as well as the current values. Modes similar to those noted for dimers [15,16] are easily excited and are evident for higher values of $\Gamma$ if shorter-length rods are used. We observe an *abrupt* transition from periodic or near-periodic behavior to stochastic motion as $\Gamma$ is increased. If $L/d>4$, the motion above the transition appears to be stochastic in nature for all higher values of $\Gamma$. The onsets for the stochastic motion were studied over rod lengths 6–21 mm and frequencies from 20 to 120 Hz. For the 3.2, 2.4, and 1.0 mm diameter stainless steel rods they lie in the ranges $\Gamma=1.03-1.13$, $\Gamma=1.10-1.20$, and $\Gamma=1.14-1.24$, respectively. However, for $L/d<4$ and for lower frequencies of vibration, episodes of low-angle near-periodic motion occur between more extended periods of stochastic oscillation for a range of $\Gamma$ above the onset, the phenomenon of intermittancy [10]. For very short rods the dynamics only become continuously stochastic at considerably higher values of $\Gamma$ than that of the first observation of stochastic motion.

We have used numerical simulations to study in some detail the onset of this stochastic behavior. Using the MD model we observe a number of periodic or near-periodic modes both for values of $\Gamma$ just above unity, and for values below unity if motion has been initiated by taking $\Gamma$ above unity and then reducing its value. This is as observed in experiment. If vibration is abruptly applied or if the vibratory conditions are changed, the motion generally settles into one of these modes after a number of bounces. For any particular rod, the equilibrium mode observed is dependent not only upon the current values of frequency and $\Gamma$ but upon the recent history of these variables. At lower values of $\Gamma$, the periodic modes noted by Dorbolo *et al.* for dimer motion [15,16] are common, including the symmetrical mode in which each end of the rod bounces in turn and the asymmetric slip-stick mode in which the rod moves across the surface.

At values of $\Gamma$ above unity a number of other modes are frequently encountered. One of these is an asymmetric mode in which one end of the rod contacts the surface twice at different angles followed by the other end touching, this sequence of three bounces being repeated. The mode may be periodic, the angles repeating exactly, or it may be near-periodic the contact angle showing a small variation about a mean. Other near-periodic modes involving longer sequences of closely repeated bounces are found. During one type a sequence of $2n$ bounces occurs. There is a sequence of $n$ distinct angles of contact involving the two ends of the rod. This is followed by a mirrored sequence of $n$ bounces involving the opposite ends of the rod. The whole sequence of $2n$ bounces repeats closely but not exactly, the contact angles showing slight variations about their mean values. These longer sequences are commonly seen in simulation but more difficult to identify in laboratory experiments.

If $\Gamma$ is slowly increased, the simulated motion abruptly changes from periodic or near-periodic to acquire a stochastic nature, as noted from experiments. At the same time, the impact angles increase appreciably. A typical example of such a transition is shown in Figs. 1(a) and 1(b), for a rod of length 15.2 mm, and $e_n=0.95$, vibrated at 60 Hz. The data of this figure were obtained from MD simulation as follows. For a number of values of $\Gamma$ between 1.0 and 2.3 the rod was dropped from a small height, being initially tilted at a small angle to the surface. Bouncing motion was then allowed to develop for 60 s to remove the influence of the initial conditions. The impact angles $\theta$ of a number of following bounces were then recorded and plotted against $\Gamma$. It may be seen from Fig. 1(b) that at small values of $\Gamma$ the motion principally involves only a few discrete impact angles, corresponding to periodic or near-periodic behavior. A detailed examination of this and similar data shows that both near-periodic three-bounce asymmetric modes and $2n$ modes with $n=4-6$ are common. The impact angles are low. However, it may be seen that at $\Gamma=1.219$ an abrupt change takes place. Above this value of $\Gamma$ the motion loses its periodic or near-periodic character and the motion adopts a stochastic character, a broad range of angles being involved. The stochastic behavior no longer depends upon the past history of frequency and $\Gamma$ but only upon the current values. Above the onset the behavior is uniformly stochastic save for a few very narrow bands of periodic or near-periodic behavior that occur for selected initial conditions and for values of $\Gamma$ not far above the transition to stochastic behavior; such behavior is seen in Fig. 1(a) for $\Gamma\sim1.65$. However, we have been unable to observe in experiment these extremely narrow bands. This

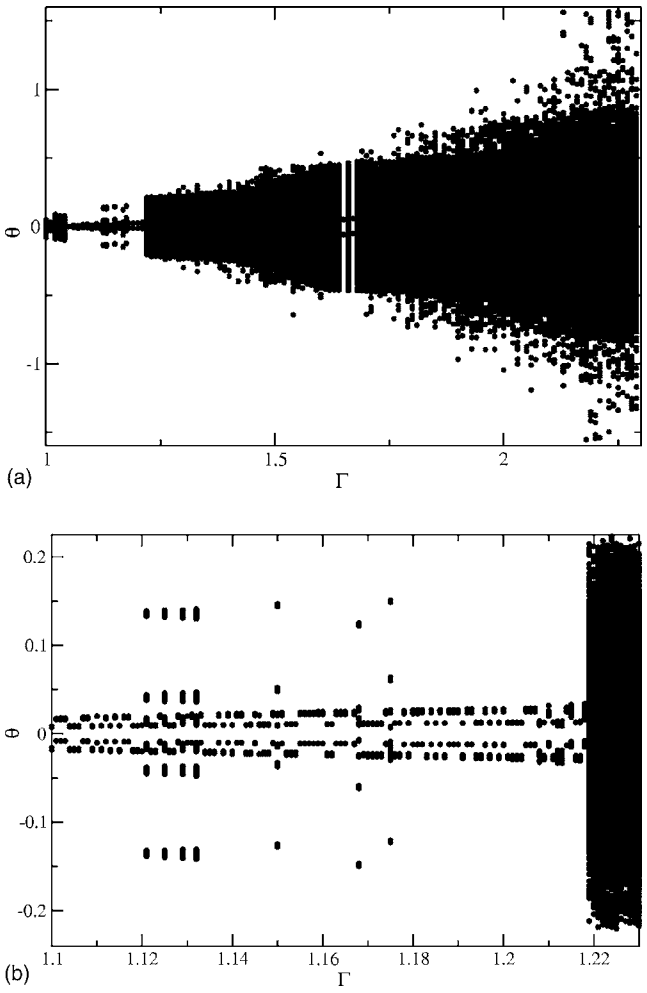


FIG. 1. The impact angles found at a set of values of Γ, plotted versus Γ, for a rod of length 15.2 mm and $e_n$=0.95, vibrated at a frequency of 60 Hz. The data were obtained from numerical simulation using the methods and parameters described in the text and show the transition from periodic or near-periodic behavior to stochastic dynamics. The onset of stochastic motion at Γ=1.219 is clearly evident. (b) is an expanded view of (a), covering the Γ range from 1.1 to 1.225.

may be due to geometric imperfections in the rods.

In MD simulation we find that the onset of stochastic motion occurs at values of Γ which vary only slowly with frequency and rod length over the ranges studied, 20–120 Hz, and 6–21 mm, respectively. The value of Γ at onset increases with decreasing $e_n$. Using values for $e_n$(bounce) corresponding to the 2.4-mm-diameter rod the onsets typically lie in the range $1.15<\Gamma<1.28$.

We note that, since our simple model does not contain the rod diameter, it cannot be expected to capture the switching between stochastic and near-periodic behavior observed experimentally for short rods. In this paper we are interested in the regions of fully stochastic rod dynamics and we only touch lightly upon measurements made at low frequencies and low values of Γ for rods such that $L/d<4$.

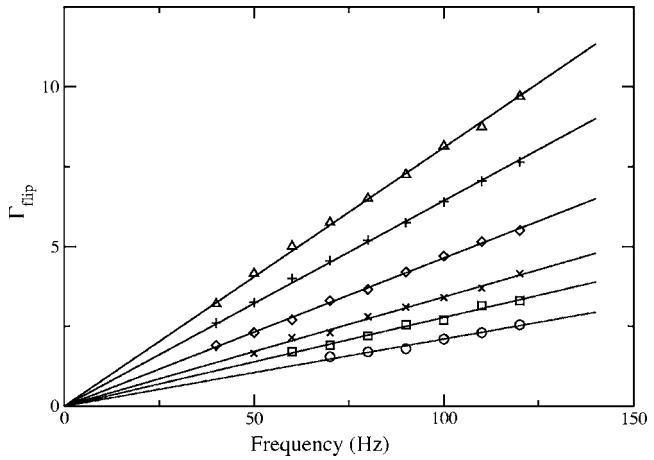


FIG. 2. The experimentally observed values of $\Gamma_{flip}$ for which the mean flipping rate is one per minute, as a function of frequency for rods having a diameter of 2.4 mm. The rod lengths are as follows: Δ 21.1 mm, +18.4 mm, ◇ 15.2 mm, ×11.5 mm, □ 9.3 mm, and ○ 5.8 mm. For the 5.8 and 9.3 mm rod lengths we observe periods of low-angle near-periodic motion between longer periods of stochastic motion at low frequencies. Where this occurs no data are shown.

### B. The observation of flipping

One convenient feature of the rod dynamics that may be obtained both from numerical simulation and from experimental observation is the rate of occurrence of end over end flipping during flight. We observe both in simulation and in experiment that the rate of flipping, in which the rod passes through the vertical position, increases very rapidly with increasing Γ (Fig. 1). It is therefore very easy to determine that value of Γ, $\Gamma_{flip}$, at which the mean flipping rate acquires any particular value. For convenience we choose a mean flipping rate of one flip per minute.

Figure 2 shows the experimentally determined values of $\Gamma_{flip}$ for this flip rate as a function of frequency and for a number of rod lengths each having a diameter of 2.4 mm. We have not included low-frequency data for the shortest rod lengths for which continuous stochastic behavior is not found. It may be seen that for each $L$ the data closely follow a straight line which passes through the origin. This suggests that the flipping rate is proportional to the peak platform velocity. $\Gamma_{flip}$ increases more rapidly than linearly with rod length $L$. Data having the same features have also been obtained for rods of diameter 1.0 and 3.2 mm. The values of $\Gamma_{flip}$(100 Hz) corresponding to a mean of one flip per minute measured at 100 Hz, have been plotted against rod length in Fig. 3. Here it may be clearly seen that for each diameter of rod, $\Gamma_{flip}$(100 Hz) increases somewhat more rapidly than linearly with rod length and that the data for smaller rod diameters lie on a higher curve.

The data corresponding to Fig. 2 but obtained from numerical simulation using the MD model are shown in Fig. 4. Figure 4 also shows, as an inset, the number of flips within a 600 s period, $N_F$, plotted against Γ for $L$=15.2 mm and each of three frequencies. It is seen that $N_F$ increases very rapidly with Γ making clear the ease with which $\Gamma_{flip}$ may be

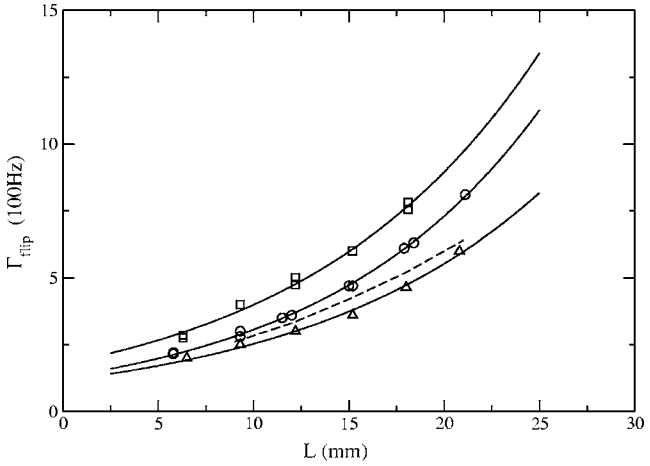


FIG. 3. The observed values of $\Gamma_{flip}$ for which the mean flipping rate is once per second at a frequency of 100 Hz, plotted against rod length for three rod diameters: □ 1.0 mm, ○ 2.4 mm, and Δ 3.2 mm. The solid lines are guides to the eye. The data from MD simulation using the experimental $e_n$ (bounce) data for 2.4 mm diameter rods are shown as a broken line.

determined either in experiment or in simulation. In Fig. 4 the restitution values $e_n$(bounce) have been used. For each rod length, $\Gamma_{flip}$ varies almost linearly with frequency, as was true for the experimental data. At any particular frequency $\Gamma_{flip}$ increases slightly more rapidly than linearly with rod length, as is clear when the $\Gamma_{flip}$(100 Hz) numerical data from Fig. 4 are plotted against rod length in Fig. 3 (broken line). From simulation the reason for this behavior is evident. If $e_n$ is kept constant then the relationship between $\Gamma_{flip}$(100 Hz) and rod length is approximately linear. However, we have noted from experiment that $e_n$(bounce) falls

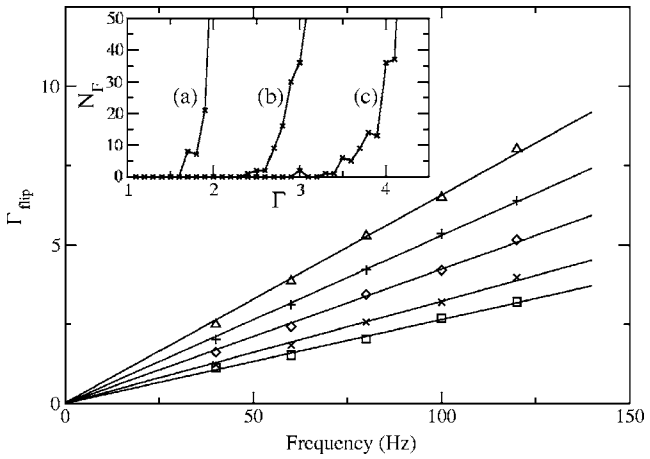


FIG. 4. The values of $\Gamma_{flip}$ for which the mean flipping rate is one per minute obtained from MD simulation, as a function of frequency. The rod lengths are as follows: Δ 21.1 mm, +18.4 mm, ◇ 15.2 mm, ×11.5 mm, and □9.3 mm. In the simulations $\mu$=0.15 and the measured $e_n$ (bounce) for rods of diameter 2.4 mm have been used. The inset shows the number of flips, $N_F$, found in a period of 600 s versus Γ for 40 (a), 60 (b), and 80 Hz (c), illustrating the abruptness of the dependence upon Γ. The inset data are for $L$=15.2 mm.

with increasing rod length (Table I); this has been included in our simulations. Since increased dissipation increases the value of Γ needed to cause flipping, the data of Fig. 3 show a dependence on rod length which is stronger than linear.

The data of Fig. 3 for the 2.4-mm-diameter rods suggest that better agreement between simulation and experiment may be obtained by somewhat increasing the dissipation in simulation, by an amount that depends upon rod length. The effective coefficient of restitution of a rod is known to vary somewhat with impact angle [22]. We therefore chose to decrease $e_n$, while the friction coefficient $\mu$ retains its measured value. Bringing simulation into agreement with the experimental data of Fig. 2 in this way offers the new set of $e_n$, $e_n$(flip), given in Table I. These values offer an overall improvement in the predictions of the MD model and will be used in what follows. The improvement offered by $e_n$(flip) over $e_n$(bounce) in predicting dynamics involving a wide range of impact angles is to be expected since the flipping process itself involves a wide range of impact angles.

### C. The statistics of the times between impacts

On each occasion when the rod impacts the vibrating mirror, the piezoelectric transducer attached to the rear of the mirror picks up a transient wave form which lasts for about 1 ms. These signals have been used to obtain the statistical distribution of times between adjacent collisions as follows. The transducer output is passed through a high-pass filter to remove traces of the vibratory wave form and is then accessed by an analysis computer. The computer detects when the voltage wave form rises through a level above the electronic noise, and notes this as an impact time. After a dead time of 1.5 ms, just longer than an individual impact transient, impact detection resumes. A succession of impact times are sent to a file for subsequent analysis. In particular, sequences of about $10^5$ impacts are analyzed to provide the probability $P_\tau(\tau)d\tau$ of times between successive impacts, $\tau$, in the range $\tau$ and $\tau+d\tau$. Note that this technique cannot be used to measure times between impacts of less than the dead time.

Figure 5 shows typical experimental probability distributions, plotted on a log-linear scale. Data for $L$=11.5 mm, $f$=50 Hz, and Γ=2.5 and for $L$=21.1 mm, $f$=50 Hz, and Γ =3.25 are shown. Rods of diameter 2.4 mm were used. In each case $P_\tau(\tau)$ is seen to fall increasingly rapidly as $\tau$ is increased. The continuous lines are fits to the Gaussian function

$$P_\tau(\tau) \sim \exp\left[-\left(\frac{\tau}{\tau_0}\right)^2\right], \tag{1}$$

where $\tau_0$ is an appropriate constant. In each case the fit is not perfect and the data not only lie above the Gaussian form for small values of $\tau$, but show significant oscillatory fluctuations about the Gaussian trend at higher values of $\tau$. We have investigated the experimental behavior for many values of $L$, Γ, and $\omega$ and find that in each case the higher-$\tau$ behavior may approximately be fitted to Eq. (1), but that in each case there are significant oscillatory deviations from this form. Figure 5 also shows the predictions of the MD model using

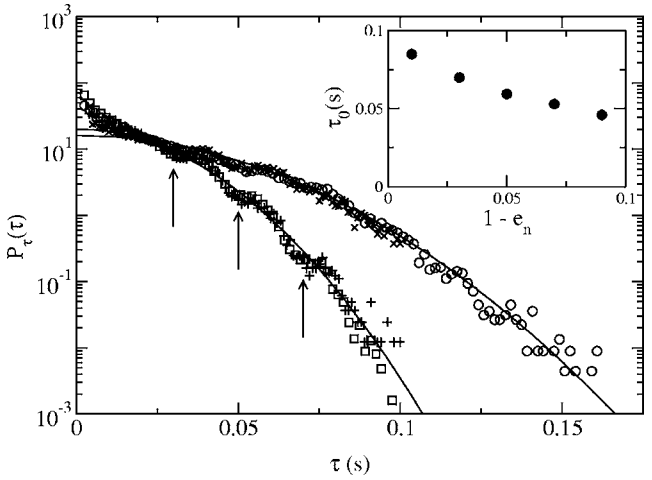


FIG. 5. The probability distribution $P_\tau(\tau)$ of the times between successive impacts, $\tau$, plotted on a log-linear scale. The experimental data for $L=11.5$ mm, $f=50$ Hz, and $\Gamma=2.5$ are shown as $\times$, while the corresponding simulation data are shown as $\bigcirc$. The experimental data for $L=21.1$ mm, $f=50$ Hz, and $\Gamma=3.25$ are shown as $+$, while the corresponding simulation data are shown as $\square$. The continuous lines are fits to the higher-$\tau$ data using the Gaussian expression Eq. (1). The arrows indicate structure that is separated in $\tau$ by the period of vibration. The inset shows, from simulation, the effect on $\tau_0$ of varying $1-e_n$, keeping all other parameters constant.

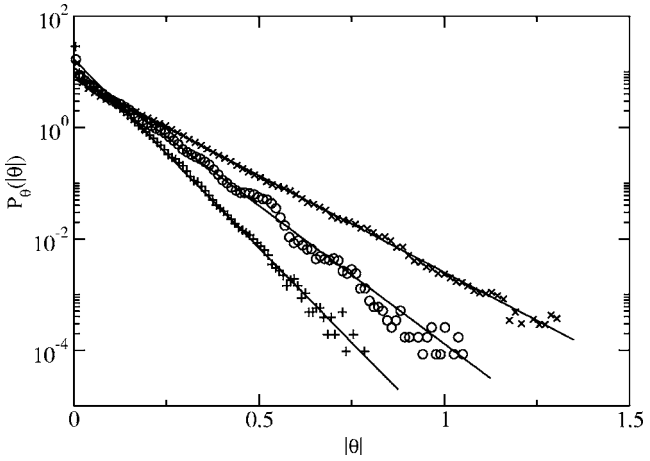


FIG. 6. The probability $P_\theta(|\theta|)$ of observing an impact angle $\theta$ plotted on a logarithmic scale against $|\theta|$. The data have been obtained from numerical simulation using the MD model. The $+$ data are for $L=21.1$ mm, $\Gamma=4.0$, and 90 Hz, the $\bigcirc$ data are for $L=15.2$ mm, $\Gamma=2.25$, and $f=70$ Hz and the $\times$ data are for $L=15.2$ mm, $\Gamma=3.0$, and $f=70$ Hz. The straight lines are fits of the tails of the distributions to Eq. (3).

$e_n=e_n$(flip). It may be seen that the model not only predicts the general trend of the data very well, but also reproduces much of the oscillatory structure. This agreement gives us further confidence in the use of our model.

The oscillatory structure found in $P_\tau(\tau)$ is always found to occur at values of $\tau$ separated by the period of vibration. This may be seen from Fig. 5, where the arrows indicate dips in the data separated by 0.02 s, the period of 50 Hz vibration. Thus, even in the stochastic regime there is some correlation between the impact times and the motion of the platform. This influence weakens at higher $\Gamma$ but is always present. This mirrors similar correlations found in the behavior of the bouncing ball [5].

Over the full range of rod lengths that we have studied and from 40 to 120 Hz the Gaussian form fits the general trend of the data well enough for the functional dependence of $\tau_0$ to be determined. We find from experiment and simulation the approximate dependence

$$\tau_0 = C_\tau \frac{a\omega}{gD(e_n,\mu)}. \tag{2}$$

Here $C_\tau$ is a numerical constant and the function $D$ is a dimensionless damping parameter. To within the accuracy that we can fit Gaussian expression Eq. (1) to simulation data there is no significant dependence of $\tau_0$ upon rod length over the range that we have used.

The damping parameter $D$ increases monotonically with $1-e_n$ and, for low values of $\mu$, with $\mu$. However, it is a complicated function of these two variables, and is not linear in either, except at vanishingly small values of the dissipation. The inset to Fig. 5 shows the corresponding variation of $\tau_0$ with $1-e_n$, keeping all other parameters fixed.

### D. The statistics of the angles of impact

Both in experiment and in simulation we observe a transition from motion involving just a few discrete impact angles to motion described by a broad range of angles above the threshold for stochastic behavior. The range of impact angles broadens as $\Gamma$ is further increased, as may be seen in Fig. 1(a). We have studied, in MD simulation, the stochastic nature of the motion seen above the transition for a wide range of the system parameters and find that, in each case, the distribution of angles is continuous. We obtain the probability distribution $P_\theta(|\theta|)d\theta$ of the impact angle $\theta$ lying in the range $\theta$ to $\theta+d\theta$. If the logarithm of the probability $P_\theta(|\theta|)$ of observing an impact is plotted against $|\theta|$ behavior close to linear is widely observed except for very low impact angles. That is, $P_\theta(|\theta|)$ may be adequately described by

$$P_\theta(|\theta|) \sim \exp\left(-\frac{|\theta|}{\theta_0}\right), \quad |\theta| < \frac{\pi}{2}, \tag{3}$$

where $\theta_0$ is a function of the system parameters. The usual definition of impact angle implies a folding of the distribution about $\theta=\pi/2$. Deviation from exponential form will therefore occur as $|\theta|$ approaches $\pi/2$. Figure 6 shows $\log_{10}(P_\theta(|\theta|))$, plotted against $|\theta|$ for three sets of the system parameters. In each case $g=9.81$ ms$^{-2}$, $\mu=0.15$, and the values of $e_n$(flip) given in Table I appropriate to the rod length have been used. For the two sets of data shown, that is, for $L=21.1$ mm, $\Gamma=4.0$, $f=90$ Hz and for $L=15.2$ mm, $\Gamma=3.0$, $f=70$ Hz, the behavior is close to linear over several decades of $\log_{10}(P_\theta(|\theta|))$, except at very low angles where the simulation data display an excess of low-angle collisions over the exponential form. Statistical behavior of this form is widely

observed. We have used the MD model to determine the dependence of the constant $\theta_0$ upon the principal parameters of the problem and conclude that the impact angle behavior is adequately described by

$$\theta_0 = C_\theta \frac{g(\Gamma - 1)}{\omega^2 L D'(e_n, \mu)}, \tag{4}$$

where $C_\theta$ is a constant and $D'(e_n, \mu)$ is a dimensionless function describing the impact damping of the rod. Again $D'$ is a complicated function of $e_n$ and $\mu$.

While, except for very low impact angles, the impact statistics broadly follow Eq. (3) for a wide range of the system parameters, a closer examination shows fine structure deviations from this mean behavior. At lower values of $\Gamma$, for shorter rods, and for greater impact damping this structure may be pronounced. Figure 6 also shows data for $L=15.2$ mm, $\Gamma=2.25$, and $f=70$ Hz. While the data show a broadly linear trend, following the dependence just given, steplike structure is now very evident. We believe that this structure results from the correlation between the times of bouncing and the phase of the platform vibration, noted in our studies of the time between bounces.

It is also interesting to consider the extent to which successive impact angles $\theta$ are correlated. This may be investigated through the correlation parameter $Q(m)$ given by the expression

$$Q(m) = \frac{(1/N)\sum_1^N \theta_n \theta_{n+m} - \left((1/N)\sum_1^N \theta_n\right)^2}{(1/N)\sum_1^N \theta_n \theta_n - \left((1/N)\sum_1^N \theta_n\right)^2}. \tag{5}$$

The sum is over the impacts within a sequence of $N$ impacts. We find that the dependence of $Q(m)$ upon $m$ is usually close to exponential; $Q(m) \sim (1/m_0)\exp(-m/m_0)$. We find that $m_0$ is not a strong function of parameters such as frequency and $\Gamma$, and is of order $m_0 \approx 6-10$. Correlation is lost typically over six to ten bounces.

### E. The energy probability distributions

A bouncing thin rod moving in two dimensions has two translational degrees and one rotational degree of freedom. We now consider in simulation the probability distributions of the total energy and the energy associated with each degree of freedom. In our simulations we have considered the rod to have unit mass; the energies quoted are therefore also per unit mass. For a particular rod length, frequency, and $\Gamma$, a MD simulation was allowed to run until the initial conditions no longer influenced the motion. The values of the three energies $E_x$, $E_z$, and $E_{rot}$ found just after each of a large number of subsequent collisions were then noted and the corresponding energy distribution functions $P_{tot}(E_{tot})$, $P_x(E_x)$, $P_z(E_z)$, and $P_{rot}(E_{rot})$ deduced. Here $E_x = \frac{1}{2} m v_x^2$ is the kinetic energy associated with the motion of the center of mass at velocity $v_x$ in the horizontal direction, $x$. Correspondingly, $E_{rot} = \frac{1}{2} I \Omega^2$ is the energy associated with rotation, where $\Omega$ is the angular velocity. These energies are constant during flight. In the case of the vertical direction $z$, it is the sum of the kinetic energy $\frac{1}{2} m v_z^2$ and the potential energy in Earth's gravity, $mgz$, which is constant during flight. Here $z$ is the height of the center of mass of the rod with respect to some chosen reference height. We take $E_z$ to be the kinetic energy immediately following collision since the potential energy associated with the variable height of the impact point is negligible [5]. The total energy $E_{tot}$ is then the sum of the three kinetic terms that we have just identified. It is possible to define two types of energy probability distribution. The first considers the probability distribution of the energies that occur following collision. The second considers the probability distribution of the energies throughout time and involves weighting the energy following collision by the time to the next impact. Following Warr *et al.* [5] we consider the first, unweighted type of distribution here.

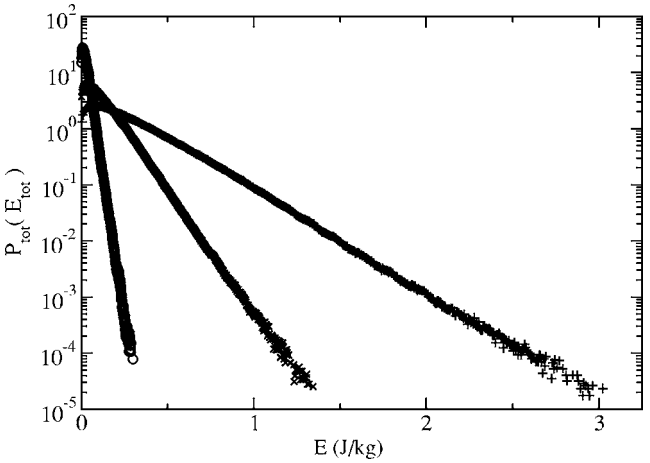


FIG. 7. The total energy probability distribution obtained from simulation plotted on a log-linear scale against total energy for a rod of length 15.2 mm, $f=50$ Hz, $\mu=0.15$, $e_n=0.937$, and for $\Gamma=3.0$ (○), 6.0 (×), and 9.0 (+).

First we consider the total energy probability distribution $P_{tot}(E_{tot})$. Some typical MD data are shown in Fig. 7, here for $L=15.2$ mm, $f=50$ Hz, and three values of $\Gamma$. It is seen that in each case $P_{tot}(E_{tot})$ falls at low energies. We have been unable to find a simple functional form that satisfactorily fits the data over the entire range. However, the high-energy tail can be fitted to a simple exponential,

$$P_{tot}(E_{tot}) \sim \exp\left[-\left(\frac{E_{tot}}{E_0}\right)\right], \tag{6}$$

where $E_0$ is a constant. We have carried out MD simulations for a wide range of the system parameters and fitted the data to Eq. (6) in each case in order to determine the factors upon which $E_0$ depends. It is found approximately that

$$E_0 = C_E \frac{a^2 \omega^2}{D''(e_n, \mu)}, \tag{7}$$

where the dissipation function $D''$ is again a complicated function of $e_n$ and $\mu$. There is no appreciable dependence of $E_0$ upon gravity or upon the rod length. The Gaussian form of flight-time distribution, Eq. (1), is consistent with the

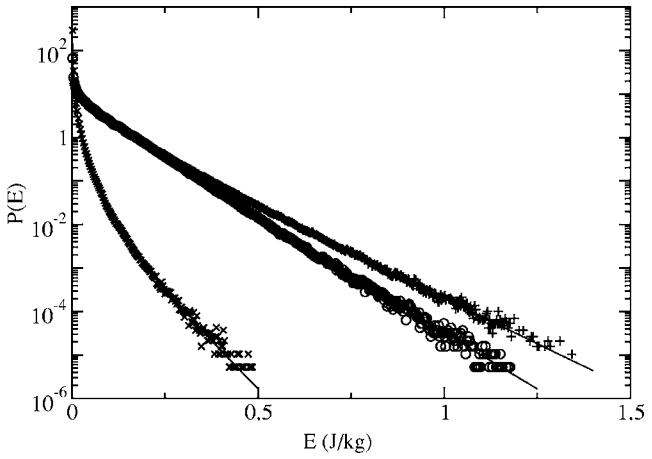


FIG. 8. The functions $P_x(E_x)$, $P_z(E_z)$, and $P_{rot}(E_{rot})$ obtained from simulation plotted on a log-linear scale against their corresponding variables for the case of $L=15.2$ mm, a frequency of 50 Hz, and $\Gamma=6.0$. The $x$ data are shown as $\times$, the $z$ data as $+$, and the rotational data as $\bigcirc$. The lines are fits to the data using Eq. (8).

observed Boltzmann tails of the energy distributions, as flight times scale linearly with launch velocities.

Typical results for the corresponding probability distribution functions $P_x(E_x)$, $P_z(E_z)$, and $P_{rot}(E_{rot})$ are shown in Fig. 8. In each case the probability of observing a given energy has a sharp *maximum* at zero energy and falls rapidly as energy increases. A fit to the data using a form

$$P(E) \sim (E+\delta)^{-\alpha} \exp\left[-\left(\frac{E}{E_0'}\right)\right] \tag{8}$$

is also shown on the figure. In each case a good fit may be obtained over the entire range, the parameter $\alpha$ taking the values 0.5, 0.2, and 2.0 for vertical translational, rotational, and horizontal translational energies, respectively. The cutoff parameter $\delta$ takes corresponding values 0.005, 0.001, and 0.0015 in units of J kg$^{-1}$. These cutoffs are necessary as the probabilities have nonzero values for $E=0$.

It is noteworthy that the distribution function for the total energy dips at zero energy, while the distribution functions for the three components exhibit maxima. This demonstrates strong correlations between the energy components. When one component is high, the others are likely to be small. There is a very low probability of all three components being large at the same time. A detailed study of the MD data confirms this correlation.

Finally we consider, using data from simulation, the proportions of energy associated with the three degrees of freedom of the rod. This may be determined from the energies following collision by taking averages of $E_x$, $E_z$, and $E_{rot}$ over very many collisions. It is then found that the proportions of the energies associated with horizontal, vertical, and rotational motion are typically in the proportions 2:54:44. These ratios only vary weakly with the system parameters. Alternatively it is possible to consider the time-averaged proportions, in which an energy after collision is weighted by the time to the next impact. The corresponding proportions are then about 3:77:20. The difference between these two sets of ratios indicates a strong correlation between the energies and the times between impacts.

Thus it may be seen that the mean energies following impact are almost equally distributed between rotation and vertical center of mass motion, there being far less energy associated with horizontal motion. However, if time-averaged energies are considered then the energy associated with vertical motion dominates the rotational energy. The time averaged energy of horizontal motion is still a very small proportion of the whole.

## V. DISCUSSION

A long rod is a geometrically simple object but the current study has shown that the high-energy dynamic behavior of a rod when bounced upon a vertically vibrating surface is complex. We have studied this behavior both in experiment and in simulation. It has been shown that a MD model is capable of describing quantitatively much of the experimentally observed behavior provided that the friction and restitution parameters are suitably chosen. This model has then been used to study those features that are more difficult to observe experimentally.

We have shown that the rod dynamics change from being periodic or near periodic to being stochastic in nature above a threshold vibration amplitude. This behavior is commonly found in impact-oscillator systems [12]. In simulation there are narrow ranges of $\Gamma$ above this threshold where narrow windows of periodic motion are found. In experiment stochastic behavior is observed for all higher $\Gamma$, probably due to small imperfections in the rod geometry. We have studied the probability distributions for various properties such as the time between impacts, the angle of impact, and the energies. The fine structures observed in these distributions for values of $\Gamma$ above the onset of stochastic behavior reduce as $\Gamma$ is increased and for values substantially above threshold, reasonably smooth distributions are found. The structures are due to correlations between impact times and the phase of the platform vibration. We have then studied the way in which these distributions depend upon the system parameters such as $\Gamma$, frequency, gravity, and rod length.

What understanding do we have of these distributions? Even in two dimensions the motion of a rod involves two linear coordinates and one rotational coordinate plus the corresponding linear and angular velocities. A collision maps a set of preimpact velocities onto a postcollision velocity set. However, this mapping is complex, involving the impact angle and details of the frictional interaction with the surface. As is the case with impact oscillators in general, any analytical treatment is challenging.

It is interesting to compare the behavior that we have observed for a rod with the corresponding behavior of a spherical bouncing ball. The exponential form Eq. (6), which we have used to describe the tails of the postcollisional energy distributions, is just that used by Warr *et al.* [5] to describe the postcollisional energies of a ball over the entire energy range which they studied. Our expression for $E_0$, Eq. (7), has the same form as that used for a ball save that the

dissipation parameter for a rod has a far more complicated dependence upon $e_n$. For the simpler problem of the bouncing ball, Warr *et al.* derived a Boltzmann energy distribution by initially considering high-energy impacts and supposing that in hitting the vibrating platform knowledge of the phase of the vibration at impact is lost [5]. Collisions therefore act as a source of noise and a Langevin description of the motion can be used. An additional collision term, included since at lower energies the ball is more likely to hit the platform during upward movement than during downward movement, gives rise to a power-law prefactor. However, for the case of the bouncing rod, a detailed understanding of the low-energy collisional behavior is still lacking, due to the coupling between translational and rotational degrees of freedom. Our findings thus suggest that a Langevin description of the dynamics may still be applicable, but the additional complexity introduced by rod rotation makes this a demanding task.

## ACKNOWLEDGMENTS

We are grateful to the Engineering and Physical Sciences Research Council for support and the loan of a high-speed camera, and to the workshop staff of the School of Physics and Astronomy for their skills and enthusiasm.

[1] R. M. Everson, Physica D **19**, 355 (1986).
[2] Z. J. Kowalik, M. Franaszek, and P. Pierański, Phys. Rev. A **37**, 4016 (1988).
[3] J. M. Luck and A. Mehta, Phys. Rev. E **48**, 3988 (1993).
[4] S. Warr and J. M. Huntley, Phys. Rev. E **52**, 5596 (1995).
[5] S. Warr, W. Cooke, R. C. Ball, and J. M. Huntley, Physica A **231**, 551 (1996).
[6] S. Giusepponi and F. Marchesoni, Europhys. Lett. **64**, 36 (2003).
[7] S. Giusepponi, F. Marchesoni, and M. Borromeo, Physica A **351**, 142 (2005).
[8] P. Devillard, J. Phys. **4**, 1003 (1994).
[9] N. B. Tuffillaro, T. Abbott, and J. Reilly, *An Experimental Approach to Nonlinear Dynamics and Chaos* (Addison Wesley, New York, 1992).
[10] R. C. Hilborn, *Chaos and Nonlinear Dynamics* (Oxford University Press, Oxford, 2000).
[11] J. C. Géminard and C. Laroche, Phys. Rev. E **68**, 031305 (2003).
[12] J. Awrejcewicz, *Bifurcations and Chaos in Nonsmooth Mechanical Systems* (World Scientific, Singapore, 2003), and references therein.
[13] C. Grebogi, E. Ott, and J. A. Yorke, Phys. Rev. Lett. **48**, 1507 (1982).
[14] D. Yamada, T. Hondou, and M. Sano, Phys. Rev. E **67**, 040301(R) (2003).
[15] S. Dorbolo, D. Volfson, L. Tsimring, and A. Kudrolli, Phys. Rev. Lett. **95**, 044101 (2005).
[16] S. Dorbelo, N. Vandewalle, D. Volfson, L. Tsimring, and A. Kudrolli, *Powders and Grains 2005* (Taylor and Francis, London, 2005), p. 1335.
[17] F. X. Villarruel, B. E. Lauderdale, D. M. Mueth, and H. M. Jaeger, Phys. Rev. E **61**, 6914 (2000).
[18] D. L. Blair, T. Neicu, and A. Kudrolli, Phys. Rev. E **67**, 031303 (2003).
[19] D. Volfson, A. Kudrolli, and L. S. Tsimring, Phys. Rev. E **70**, 051312 (2004).
[20] D. E. Stewart, SIAM Rev. **42**, 3 (2000).
[21] H. Barbulescu, D. B. Marghitu, and U. Vaidya, ASME J. Eng. Mater. Technol. **125**, 368 (2003).
[22] D. Stoianovici and Y. Hurmuzlu, J. Appl. Mech. **63**, 307 (1996).
[23] H. J. Herrmann and S. Luding, Continuum Mech. Thermodyn. **10**, 189 (1998).
[24] S. Luding, Phys. Rev. E **52**, 4442 (1995).